

IC/99/62
hep-ph/9905xxx
May 1999

Additional phases induced by the supersymmetric CP phases

D. A. Demir

*The Abdus Salam International Center for Theoretical Physics, I-34100,
Trieste, Italy*

Abstract

The explicit CP violation in the MSSM radiatively induces a finite unremovable alignment between the Higgs doublets. This additional phase can be as large as the original CP phases in certain portions of the MSSM parameter space. Considering the specific case of the charginos, this additional phase is shown to induce a conceivable amount of CP violation near the would-be CP conserving points. Moreover, the CP violation in the absence of this phase is smaller than the one in the presence of it, and the former can never compete with the latter, however large $\tan \beta$ is.

1 Introduction

The Lagrangean of the Minimal Supersymmetric Standard Model (MSSM) consists of various mass parameters which are not necessarily real. Indeed, as was studied in [1, 2], after all possible rephasings of the fields there remain two physical phases which can be chosen to be those of the μ parameter ($\varphi_\mu \equiv \text{Arg}[\mu]$), and Higgs–sfermion–sfermion trilinear couplings ($\varphi_{A_f} \equiv \text{Arg}[A_f]$). Of course, in addition to these, the QCD vacuum angle θ_{QCD} and the phase in the CKM matrix δ_{CKM} are still present as in the Standard Model (SM).

When analyzing their effects on the low-energy processes one may regard these phases as given parameters in the MSSM Lagrangian [1, 2] although it is possible to realize them, for example, by embedding the SM on D-branes [3] or more general dynamical supersymmetry breaking scenarios [2, 4]. However, independent of specific high energy realizations, the low-energy Lagrangian happens to depend on several soft phases whose physical combinations can always be chosen to be those of the μ - and A -parameters. These phases have found interesting applications in various areas of the particle phenomenology: EDM's of particles [5], LSP searches [6], K - and B -physics [1, 7], electroweak baryogenesis [8], weak and electromagnetic dipole formfactors [9], and Higgs phenomenology [10, 11].

In the presence of these phases the CP-invariance of the MSSM Lagrangian is explicitly broken, and naturally, various interaction vertices get modified. Moreover, through the radiative corrections, the squared-mass matrix of the Higgs scalars assumes CP-violating elements thereby the mass-eigenstate Higgs scalars turn out to have no definite CP quantum numbers [10, 11]. Furthermore, due to CP-violation, these phases induce a finite alignment between the Higgs doublets [10, 11] which would be absent if there were no CP-violation, explicit or spontaneous [12]. This additional phase can have non-trivial effects on the interactions of charginos, neutralinos and sfermions. In what follows, its size as well as its effects on the mixing matrices of certain particles will be analyzed as a function of the supersymmetric parameter space.

In the analysis below, φ_μ and φ_{A_f} will be taken free, that is, it is assumed that the electric dipole moment constraints [1, 5] could be sidestepped by following the appropriate parameter spaces discussed in [13]. In this work, sfermions of the first two generations will be assumed degenerate and very

heavy (see the last three references in [13]) compared to the third generation sfermions. With such heavy sfermions belonging to the first two generations one can suppress the electric dipole moments of the particles in agreement with the experimental bounds.

The radiatively induced unremovable alignment between the Higgs doublets can have nontrivial effects on the chargino and neutralinos sectors. For both clarity and simplicity this work deals mainly with the chargino sector. Accordingly, analyses below will be based on the typical combinations of the chargino mixing matrices appearing in the relevant processes listed above. Section II discusses (1) the induction and size of the additional CP phase, and (2) its effects on the chargino sector. Section III concludes the work.

2 Radiatively Induced CP Phases

The MSSM Higgs sector contains two opposite-hypercharge Higgs doublets H_1, H_2 in terms of which the tree-level potential reads as follows

$$\begin{aligned} V_0(H_1, H_2) = & m_1^2 |H_1|^2 + m_2^2 |H_2|^2 + (m_3^2 H_1 \cdot H_2 + H.c.) \\ & + \frac{\lambda_1}{2} |H_1|^4 + \frac{\lambda_2}{2} |H_2|^4 + \lambda_{12} |H_1|^2 |H_2|^2 + \tilde{\lambda}_{12} |H_1 \cdot H_2|^2 \end{aligned} \quad (1)$$

where the parameters are defined by

$$\begin{aligned} m_1^2 &= m_{\tilde{H}_1}^2 + |\mu|^2, \quad m_2^2 = m_{\tilde{H}_2}^2 + |\mu|^2, \quad \lambda_1 = \lambda_2 = (g_2^2 + g_1^2)/4 \\ \lambda_{12} &= (g_2^2 - g_1^2)/4, \quad \tilde{\lambda}_{12} = -g_2^2/2. \end{aligned} \quad (2)$$

Here $m_{\tilde{H}_{1,2}}^2$ and m_3^2 are the soft supersymmetry breaking masses determining the Higgs bilinears. Since μ enters through $|\mu|^2$ only, and phase of m_3^2 is rotated away already, the potential is spanned by the real parameters only. Therefore, Higgs fields develop only real vacuum expectation values. Indeed, even if one introduces a certain alignment θ between the Higgs doublets H_1 and H_2 , tadpole equations nullify it [14]. Namely, in the minimum, the potential is to have vanishing gradients in all directions, in particular, $\partial V_0 / \partial \varphi_{1,2} = -m_3^2 \sin \theta \equiv 0$. Here and in what follows $H_{1,2}^0$ show the neutral components of the Higgs fields, and they are linearly decomposed as follows: $H_1^0 = (v_1 + \phi_1 + i\varphi_1)/\sqrt{2}$, $H_2^0 = (v_2 + \phi_2 + i\varphi_2)/\sqrt{2}$ with $v_2/v_1 \equiv \tan \beta$ and $M_W^2 = g^2(v_1^2 + v_2^2)/4$.

It is now a well-established fact that the radiative corrections to the MSSM Higgs sector are important in that the mass of the lightest Higgs gets a large correction : $\delta m_h^2 \sim M_Z^2$. This sizable radiative correction to the Higgs mass has been computed in the framework of on-shell renormalization [15], effective potential approach [16], and RGE-improved one- and two-loop Higgs potential [17] with differing precisions and approximation methods. Here, for convenience, effective potential approximation will be followed as in [10] where the entire one-loop effects of the MSSM particle spectrum were approximated by the dominant top quark and top squark loops. This approximation is good for picking up phase-dependent dominant terms as long as very large values of $\tan \beta$ are avoided: $\tan \beta \lesssim 40$. If larger $\tan \beta$ values are considered bottom-sbottom and tau-stau loops start dominating, and the approximation adopted here fails. In what follows, analytic results of [10] will be frequently referred to avoid unnecessary repetitions.

When the one-loop corrections are added to the tree-level potential (1), it is seen that $\partial V / \partial \varphi_{1,2}$ no longer vanish; hence, one has to redefine the Higgs doublets with a relative phase between them, say, $H_1 \rightarrow H_1, H_2 \rightarrow e^{i\theta} H_2$ with which now $\partial V / \partial \varphi_{1,2} \equiv 0$ gives [10]

$$\sin \theta = -\beta_{h_t} \frac{|\mu| |A_t|}{M_A^2 \sin 2\beta} \sin \gamma f(m_{\tilde{t}_1}^2, m_{\tilde{t}_2}^2) \quad (3)$$

where $\beta_{h_t} = h_t^2 / 16\pi^2$, $\gamma = \varphi_\mu + \varphi_{A_t}$, and $M_A^2 = -m_3^2 / (\sin \beta \cos \beta)$ corresponds to the tree-level pseudoscalar mass in the CP-conserving theory. Finally, the loop function f is defined by

$$f(x, y) = -2 + \log \frac{xy}{Q^4} + \frac{y+x}{y-x} \log \frac{y}{x} \quad (4)$$

which has an explicit dependence on the renormalization scale Q . The stop masses $m_{\tilde{t}_{1,2}}$ in (3) are given by

$$m_{\tilde{t}_{1(2)}}^2 = \frac{1}{2} \left(M_L^2 + M_R^2 + 2m_t^2 - (+)\Delta_{\tilde{t}}^2(\gamma) \right) \quad (5)$$

where $\gamma = \gamma_\mu + \gamma_{A_t}$, and

$$\Delta_{\tilde{t}}^2(\gamma) = \sqrt{(M_L^2 - M_R^2)^2 + 4m_t^2(|A_t|^2 + |\mu|^2 \cot^2 \beta - 2|\mu||A_t| \cot \beta \cos \gamma)} \quad (6)$$

Before going into details it is convenient to discuss the role of the parameter M_A in eq. (3). As mentioned just after (3) it is the tree level pseudoscalar

mass in the CP-conserving theory, that is, it does not include the loop corrections. Indeed, as derived in [10], the squared-mass matrix of the Higgs scalars depends on the combination $\tilde{M}_A^2 = M_A^2(\sin(\gamma - \theta)/\sin \gamma)$ instead of M_A^2 . However, even \tilde{M}_A is itself away from representing the mass of any of the scalars; there are further radiative corrections determining the Higgs masses and mixings. Although \tilde{M}_A is an appropriate fundamental variable for the Higgs sector, in studying the relative phase θ it is convenient to take M_A fundamental as this causes no physical difficulty as long as one deals with variables having explicit dependence on the renormalization scale Q .

The second important thing to be noted is the explicit Q dependence of θ . Usually the explicit Q dependence is assumed to cancel with the implicit Q dependencies of $\tan \beta$ and m_3^2 [16]. Besides, in analyzing the Higgs sector this explicit Q dependence is embedded into the quantity \tilde{M}_A mentioned above. However, in general, all tree-level quantities are to be interpreted as evaluated at the scale Q . Indeed, the logarithms produced by the renormalization group evolution of the tree level quantities from GUT to the weak scale have been shown to slow down the Q dependence coming from the effective potential [18]. In the following Q will be taken at the weak scale, that is, $Q \sim m_t$. When the supersymmetric mass parameters are around m_t , as will be the case in the following numerical studies, the Q -dependence of θ will be weak.

For further progress, it is convenient to clarify the dependence of $\sin \theta$ on various MSSM parameters on the right-hand side of (3):

1. $\sin \theta$ vanishes identically once a CP-conserving point is approached, that is, $\gamma \rightarrow 0, \pi$. Therefore, θ is solely induced by the CP violating phases, and vanishes whenever the CP-invariance is restored.
2. $\sin \theta$ varies as $1/M_A^2$, and thus, it is diminished in the decoupling regime [19].
3. Putting aside the effects of the loop function, $\sin \theta \propto \tan \beta / \sin^2 \beta$ so that it grows with increasing $\tan \beta$.
4. For large $\tan \beta$, γ dependence of $\Delta_{\tilde{t}}^2(\gamma)$ weakens and $\sin \theta$ becomes proportional to $\sin \gamma$.

5. $\sin \theta \propto |\mu||A_t|$, and the latter could, in principle, be large. Here the only constraint on $|\mu|$ and $|A_t|$ arises from the requirement of keeping electric and color symmetries unbroken [20]. This requires the light stop squared-mass be positive, or best, be above the existing experimental lower bounds.
6. As the detailed discussions in [10, 11] show masses as well as the couplings of the MSSM particles now depend on the phase γ , as a result, various constraints on the parameter space, derived for $\gamma = 0$, do not necessarily hold for finite γ . Thus, one can, in fact, relax certain mass bounds especially in the Higgs sector due to strong γ dependence of their masses and couplings, and also their indefinite CP quantum numbers.

In the light of above-listed properties, one concludes that $\sin \theta$ could be of the same order as $\sin \gamma$ if

$$\frac{|\mu||A_t|}{M_A^2 \sin^2 \beta \cos \beta} f(m_{\tilde{t}_1}^2, m_{\tilde{t}_2}^2) \sim \frac{16}{3} \pi^2. \quad (7)$$

To see if this rough condition is satisfied it is convenient to have a numerical study of it. However, MSSM parameter space is too wide to cover fully so it is necessary to choose certain values for the parameters meeting, at least, some of the related phenomenological constraints. The induced phase θ will eventually find applications in various processes mentioned in the Introduction, in particular, in electroweak baryogenesis [8] and K and B -meson studies [7] both of which require the soft parameters as well as the μ parameter be around the weak scale. To illustrate a conservative case one can take, for example, $M_{\tilde{L}} = M_{\tilde{R}} = 2 \cdot M_Z$ with $m_{\tilde{t}_1} \geq M_Z$. Such low values of the stop soft masses together with the lower bound on the light stop mass constrains the stop left-right mixings considerably. Hence, $|A_t|$ and $|\mu|$ parameters are rather restricted. Despite these constraints, if one can find a solution giving $|\theta| \sim \mathcal{O}(1)$, then it is guaranteed that for higher values of the stop left-right mixings a satisfactory solution will exist. The natural renormalization scale is the weak scale; hence the choice $Q^2 = m_t^2$. Q will always be kept at this value irrespective of the variations in other parameters. Apart from these assignments of the parameters, to guarantee that $\sin \theta$ is really large in some region of the parameter space, it is necessary to compare it with maximal

value of $\sin \gamma$, that is, $\gamma = \pi/2$. In the analysis of θ below, the remaining parameters $\tan \beta$, M_A , $|A_t|$ and $|\mu|$ will be varied freely except for the fact that all mass parameters, including the light stop mass, will be required to lie above M_Z .

Depicted in Fig. 1 is the variation of $\sin \theta$ in $|A_t|/M_Z - |\mu|/M_Z$ plane for $\tan \beta = 2$ and $M_A = M_Z$. In this as well as other figures $\sin \theta = 0$ plateau *is not* the actual value of $\sin \theta$ instead it shows the *excluded region* in the $|A_t|/M_Z - |\mu|/M_Z$ plane for which either $m_{\tilde{t}_1} < M_Z$ or $|\sin \theta| > 1$. As the figure suggests, $\sin \theta$ starts with ~ -0.05 at $|A_t| = |\mu| = M_Z$, and falls to ~ -0.6 until $|\mu| \sim 6M_Z$ and $|A_t| \sim 3.2M_Z$. Here $\sin \theta$ cannot reach -1 since $m_{\tilde{t}_1}$ falls below M_Z at the boundary shown. Thus, for $\tan \beta = 2$ and $M_A = M_Z$, $|\sin \theta|$ value as large as $\sim 60\%|\sin \gamma|$ are reachable.

Fig. 2 illustrates the same quantity in Fig. 1 for $\tan \beta = 30$. Contrary to Fig. 1, here $|\sin \theta|$ exceeds unity well before $m_{\tilde{t}_1}$ falls below M_Z hence the different shapes for the onset of the forbidden regions in two figures. It is clear that this time $|\sin \theta|$ reaches unity for $|A_t| \sim |\mu| \sim 140 \text{ GeV}$. As one recalls from Item (3) in the previous page, it is the strong $\tan \beta$ dependence of $|\sin \theta|$ that causes this difference between Figs. 1 and 2.

Fig. 3 has the same conventions in Fig. 1 but uses $M_A = 2 \cdot M_Z$. As already mentioned in Item (2) in the previous page, $|\sin \theta|$ is rapidly diminished with increasing M_A . As the figure shows doubling of M_A reduces $|\sin \theta|$ from the maximal value of ~ 0.6 to 0.15 as is obvious from its M_A dependence.

Finally, Fig. 4 is for $M_A = 2 \cdot M_Z$ and $\tan \beta = 30$. As is seen, $|\sin \theta|$ hits unity before $m_{\tilde{t}_1}$ falls below M_Z . As in Fig. 2 $|\sin \theta|$ values as large as $|\sin \gamma|$ are reachable.

It may be convenient to have a comparative discussion of these four figures. That $m_{\tilde{t}_1}$ falls below M_Z determines the starting of the forbidden regions in Figs. 1 and 3. In these figures $\tan \beta = 2$ and $|\mu|$ term contribution is not suppressed at all, and $\Delta_t^2(\pi/2)$ grows rapidly with increasing $|A_t|$ and $|\mu|$ causing $m_{\tilde{t}_1}$ to approach faster to M_Z . In these two figures $|\sin \theta|$ is controlled essentially by $(|\mu||A_t|)/M_A^2$; however, $|\mu|$ and $|A_t|$ are constrained by charge and/or color breaking. Concerning this point one notes that the allowed range of $|\mu|$ and $|A_t|$ remain the same in both figures, and range of $|\sin \theta|$ follows from the value of M_A .

In Figs. 2 and 4 $\tan \beta = 30$, and $m_{\tilde{t}_1}$ remains above M_Z in a larger region than Figs. 1 and 3. This follows simply from the $\cot \beta$ suppression of the $|\mu|$ -term contribution to the stop mass-squared splitting $\Delta_t^2(\pi/2)$. In both figures starting of the forbidden region is determined by the fact that $|\sin \theta|$ exceeds unity. Hence, in both cases $|\sin \theta|$ assumes its allowed maximal value: $|\sin \theta| \sim |\sin \gamma|$. In sum, one observes that $\tan \beta$ plays a double role in determining $|\sin \theta|$: It both pushes away color and/or charge breaking boundary, and enhances $|\sin \theta|$ due to the dependence summarised in Item (3) in the previous page.

The illustrations above show that there are certain regions of the MSSM parameter space in which $|\sin \theta|$ is maximally large. As mentioned in the Introduction, this additional phase θ enters sfermion, chargino and neutralino mass matrices. To this end it is convenient to discuss first stop mass matrix. If one starts the whole analysis with a relative alignment between the Higgs doublets, as already mentioned in [10], the entire effect is just a shift of γ by θ : $\gamma \rightarrow \gamma + \theta$ in the stop mass matrix. Thus, one may regard γ at the right hand side of equation (3) as including θ already. In this sense reinsertion of θ to the stop squared-mass matrix is inconsistent because θ itself is generated by γ through (3). In sum, were it not for the charginos and neutralinos one would just redefine the angle γ with the replacement $\gamma \rightarrow \gamma + \theta$, and a particular analysis of θ would be useless. In what follows presented is a detailed discussion of the CP violation in the chargino sector.

The charginos which are the mass eigenstates of charged gauginos and Higgsinos are described by a 2×2 mass matrix [21]

$$M_C = \begin{pmatrix} M_2 & -\sqrt{2}M_W \cos \beta \\ -\sqrt{2}M_W \sin \beta e^{i\theta} & |\mu|e^{i\varphi_\mu} \end{pmatrix} \quad (8)$$

where M_2 , which is the SU(2) gaugino mass, was made real already by appropriate field redefinitions mentioned in the Introduction [1, 2]. The masses of the charginos as well as their mixing matrices follow from the biunitary transformation

$$C_R^\dagger M_C C_L = \text{diag}(m_{\chi_1}, m_{\chi_2}) \quad (9)$$

where C_L and C_R are 2×2 unitary matrices, and m_{χ_1} , m_{χ_2} are the masses of the charginos χ_1 , χ_2 such that $m_{\chi_1} > m_{\chi_2}$. It is convenient to choose the

following explicit parametrization for the chargino mixing matrices:

$$C_L = \begin{pmatrix} \cos \theta_L & \sin \theta_L e^{i\varphi_L} \\ -\sin \theta_L e^{-i\varphi_L} & \cos \theta_L \end{pmatrix} \quad (10)$$

$$C_R = \begin{pmatrix} \cos \theta_R & \sin \theta_R e^{i\varphi_R} \\ -\sin \theta_R e^{-i\varphi_R} & \cos \theta_R \end{pmatrix} \cdot \begin{pmatrix} e^{i\phi_1} & 0 \\ 0 & e^{i\phi_2} \end{pmatrix} \quad (11)$$

where the angle parameters $\theta_{L,R}$, $\varphi_{L,R}$, and $\phi_{1,2}$ can be determined from the defining equation (9). A straightforward calculation yields

$$\begin{aligned} \tan 2\theta_L &= \frac{\sqrt{8}M_W \sqrt{M_2^2 \cos^2 \beta + |\mu|^2 \sin^2 \beta + |\mu|M_2 \sin 2\beta \cos(\varphi_\mu - \theta)}}{M_2^2 - |\mu|^2 - 2M_W^2 \cos 2\beta} \\ \tan 2\theta_R &= \frac{\sqrt{8}M_W \sqrt{|\mu|^2 \cos^2 \beta + M_2^2 \sin^2 \beta + |\mu|M_2 \sin 2\beta \cos(\varphi_\mu - \theta)}}{M_2^2 - |\mu|^2 + 2M_W^2 \cos 2\beta} \\ \tan \varphi_L &= \frac{|\mu| \sin(\varphi_\mu - \theta)}{M_2 \cot \beta + |\mu| \cos(\varphi_\mu - \theta)} \\ \tan \varphi_R &= -\frac{|\mu| \cot \beta \sin \varphi_\mu + M_2 \sin \theta}{|\mu| \cot \beta \cos \varphi_\mu + M_2 \cos \theta} \end{aligned} \quad (12)$$

in terms of which the remaining two angles ϕ_1 and ϕ_2 read as follows

$$\tan \phi_i = \frac{\text{Im}[Q_i]}{\text{Re}[Q_i]} \quad (13)$$

where $i = 1, 2$ and

$$\begin{aligned} Q_1 &= \sqrt{2}M_W [\cos \beta \sin \theta_L \cos \theta_R e^{-i\varphi_L} + \sin \beta \cos \theta_L \sin \theta_R e^{i(\theta + \varphi_R)}] \\ &\quad + M_2 \cos \theta_L \cos \theta_R + |\mu| \sin \theta_L \sin \theta_R e^{i(\varphi_\mu + \varphi_R - \varphi_L)} \\ Q_2 &= -\sqrt{2}M_W [\cos \beta \sin \theta_R \cos \theta_L e^{-i\varphi_R} + \sin \beta \cos \theta_R \sin \theta_L e^{i(\theta + \varphi_L)}] \\ &\quad + M_2 \sin \theta_L \sin \theta_R e^{i(\varphi_L - \varphi_R)} + |\mu| \cos \theta_L \cos \theta_R e^{i\varphi_\mu}. \end{aligned} \quad (14)$$

The origin of the phases $\theta_{L,R}$, $\varphi_{L,R}$, and $\phi_{1,2}$ is easy to trace back. The angles θ_L and θ_R would be sufficient to diagonalize, respectively, the quadratic mass matrices $M_C^\dagger M_C$ and $M_C M_C^\dagger$ if M_C were real. As a result one needs the additional phases $\varphi_{L,R}$ which are identical to the phases in the off-diagonal entries of the matrices $M_C^\dagger M_C$ and $M_C M_C^\dagger$, respectively. However, these four phases are not still sufficient for making the charginos masses real positive due to the biunitary nature of the transformation (9); hence, the phases ϕ_1 and ϕ_2 .

Inserting the unitary matrices C_L and C_R into the defining equation (9) one obtains the following expressions for the masses of the charginos

$$m_{\chi_{1(2)}}^2 = \frac{1}{2} \left\{ M_2^2 + |\mu|^2 + 2M_W^2 + (-) [(M_2^2 - |\mu|^2)^2 + 4M_W^2 \cos^2 2\beta + 4M_W^2 (M_2^2 + |\mu|^2 + 2M_2|\mu| \sin 2\beta \cos(\varphi_\mu - \theta))]^{1/2} \right\}. \quad (15)$$

As is clear from eqs. (8)-(14) all chargino mixing parameters as well as their masses themselves depend explicitly on the phases φ_μ and θ . From such dependencies of the derived quantities one immediately infers that:

- Even if φ_μ vanishes there is still a source for CP violation due to the presence of θ .
- If both φ_μ and φ_{A_t} vanish then there remains no source for CP violation.
- As the expressions of φ_R , ϕ_1 and ϕ_2 suggest, in general, it is not possible to absorb θ into a redefinition of φ_μ .

For an analysis of the contribution of θ to CP violation in chargino sector it is convenient to form appropriate CP-violating quantities from the ones derived above. In general, when analyzing the effects of these phases on various observables, it is convenient assume a vanishing phase for the CKM matrix [22] to identify the pure supersymmetric contributions. In this context one recalls the discussions of $B \rightarrow X_s \gamma$ [23], $B-\bar{B}$ and $K-\bar{K}$ mixings [24], and EDM calculations (second and third references in [13]) in which the CP violation due to the chargino contributions depends on the particular combinations of the matrices C_L and C_R . Among all possible combinations, one can choose, for example,

$$f_i(\theta, \varphi_\mu) = \text{Im} \left\{ (C_L^\dagger)_{i2} (C_R)_{1i} \right\} \quad (16)$$

where $i = 1, 2$. In the actual applications the quantity in $\text{Im}\{\dots\}$ is multiplied by (1) the Yukawa couplings of the external fermions, (2) appropriate loop functions, and (3) the elements of the stop mixing matrix. The first two factors do not add new phases but weight the amount of CP violation. Especially the $\tan \beta$ dependence of the Yukawa couplings is important. The third factor brings the additional phase $\varphi_t = \text{Arg}[A_t - \mu \cot \beta]$ which is important for determining the total CP-violation for a particular process. The

net CP violation would be given by the first two factors times the real part of the stop contribution times $f_i(\theta, \varphi_\mu)$ plus the imaginary part of the stop contribution times the real part of the chargino contribution. Since amount of the CP violating phase coming from the stop sector does not change with finite θ , the main novelty (apart from θ dependence of various quantities such as the stop and chargino masses) is brought about by $f_i(\theta, \varphi_\mu)$. Keeping in mind these restrictions it is now time for having a numerical analysis of f_i in the parameter spaces of Figs. 1-4.

In the numerical study of $f_i(\theta, \varphi_\mu)$ the free variable will be φ_μ . The other parameters will be fixed from the parameter spaces of the Figs. 1 and 4. Thus it is convenient to introduce two parameter sets A and B

$$A = \left\{ M_{\tilde{L}} = M_{\tilde{R}} = M_2 = 2 \cdot M_Z, M_A = M_Z, |A_t| = 3.6 \cdot M_Z, \right. \\ \left. |\mu| = 6 \cdot M_Z, \tan \beta = 2, \varphi_{A_t} = 0.7 \right\}, \quad (17)$$

$$B = \left\{ M_{\tilde{L}} = M_{\tilde{R}} = M_2 = 2 \cdot M_Z, M_A = 2 \cdot M_Z, |A_t| = 3 \cdot M_Z, \right. \\ \left. |\mu| = 3 \cdot M_Z, \tan \beta = 30, \varphi_{A_t} = 0.9 \right\}, \quad (18)$$

subject to the constraints

$$\mathcal{C} = \left\{ m_{\tilde{t}_1} \geq M_Z, m_{\chi_2} \geq M_W, |\sin \theta| \leq 1 \right\}, \quad (19)$$

for any φ_μ and φ_{A_t} . Similar to the parameter spaces of Figs. 1-4 the mass parameters are chosen to lie slightly above M_Z . Such a choice for the parameter space is motivated by the phenomenological requirements as well as minimization of the scale dependence of θ . One notices that the values of the parameters $|A_t|$ and $|\mu|$ in A and B remain outside the allowed regions of Figs. 1 and 4, respectively. This does not pose a problem since these figures were formed for $\gamma = \pi/2$ whereas in the figures below CP phases will be varied over a range of values. The specific choices for the phase φ_{A_t} follow from the search strategy: One sets first φ_μ to zero and checks the variation of f_i with φ_{A_t} through its θ dependence. Generally, f_i assumes a piece-wise continuous curve with φ_{A_t} due to the violation of the constraints \mathcal{C} place to place. Then that value of φ_{A_t} closest to the origin, and for which f_i is maximum is picked up. In general, there is no *a priori* condition saying what range of values are appropriate for φ_{A_t} . However, those values of the supersymmetric phases as close as possible to a CP conserving point are interesting by themselves. In what follows, unless otherwise stated, all conditions in \mathcal{C} will be applied

irrespective of the presence or absence of the angle θ in the chargino sector. That is, even if θ is not included in the chargino sector the condition on it in \mathcal{C} will be applied in illustrating f_i .

Figs. 5-8 show the φ_μ dependence of f_i for the parameters in sets A and B in the presence (solid curves) and absence (dashed curves) of θ in the chargino sector. In each figure the dashed curve shows how big f_i would be if there were no contribution from the additional CP angle θ . Moreover, in each figure argument of f_i refers to the parameter sets A or B as is self-explanatory. For the parameter set A , f_1 and f_2 are shown in Figs. 5 and 6, respectively. In each figure the discontinuity at $\varphi_\mu \sim 0.3$ corresponds to the violation of any member of \mathcal{C} . There are such discontinuities at other values of φ_μ as well but for clarity their discussion will be given later. As expected, in the absence of θ , in each figure f_i increases linearly with φ_μ until \mathcal{C} is violated. However, due to φ_{A_t} support at finite θ , $|f_1|$ starting from its maximum at $\varphi_\mu = 0$ decreases gradually until $\varphi_\mu \sim 0.3$. Except for a small region between $\varphi_\mu = 0.27$ and $\varphi_\mu = 0.3$ $|f_1|$ for finite θ is larger than that for vanishing θ . By construction, the figure suggests that $|f_1|$ is quite large for vanishing φ_μ . Fig. 6 shows the behaviour of f_2 as in Fig. 5. In this case, solid curve is much larger than the dashed one everywhere, in particular, the solid curve starts $|f_2| \sim 0.17$ at $\varphi_\mu = 0$ and increases near 0.2 at $\varphi_\mu \sim 0.2$ beyond which it decreases gradually. Taking the arithmetic means of the curves in the relevant φ_μ interval one observes that there is an order of magnitude enhancement. The interesting thing is that for larger values of φ_μ the two curves become at most equal implying that the finite θ contribution is important.

Similar to Figs. 5 and 6, depicted in Figs. 7 and 8 are the φ_μ -dependence of f_1 and f_2 for the parameter set B . Here it is seen that the threshold value of φ_μ at which \mathcal{C} is violated is approximately one order of magnitude below the one for the parameter set A . Hence in the former the φ_μ values are closer to the CP conserving points $\varphi_\mu = 0$ than the latter. This stems mainly from the slightly large value of $\tan\beta$ which pushes $|\sin\theta|$ beyond its limits in \mathcal{C} . This effect could also be observed in Figs. 2 and 4. Again with the mean values of the curves one obtains more than an order of magnitude enhancement in f_i for finite θ . One notices that, in all four figures, there is no sign shift in f_i for finite and vanishing θ . However, relative magnitudes

of f_i change in finite θ case.

Although φ_μ values involved in Figs. 5-8 are relatively small, the φ_{A_t} value is close to unity, and thus, it is quite away from the CP-conserving point $\varphi_{A_t} = 0$. Moreover, one may wonder if f_i in the presence of θ does really dominate over the one in the absence of θ in the chargino sector. This point is important because it may happen that f_i for finite θ could be of similar magnitude as the one for vanishing θ so that the net effect of introducing θ could be just a shift in the value of φ_μ . Although the expressions for various angles in eqs. (12)-(14) guarantee that this does not happen, it may still be convenient to illustrate this point for a sample parameter space. In doing this it is appropriate to search for a region of the parameter space where both CP phases remain in close vicinity of a CP-conserving point. In this respect one can introduce the following parameter set:

$$C = \left\{ M_{\tilde{L}} = M_{\tilde{R}} = M_2 = 4 \cdot M_Z, M_A = M_Z, |A_t| = 11 \cdot M_Z, \right. \\ \left. |\mu| = 11 \cdot M_Z, \tan \beta = 2, \varphi_{A_t} = 0.052 \right\} \quad (20)$$

which is again subject to the constraint \mathcal{C} . It is obvious that now stop left-right mixings are chosen to be large in accordance with stop soft mass parameters: $|A_t| = |\mu| \sim \text{a TeV}$, and $M_{\tilde{L}} = M_{\tilde{R}} \sim 350 \text{ GeV}$. Before discussing the implications of the set C , it is convenient to see, for example, f_1 in Fig. 7 in the entire range of φ_μ to observe the competition between values of f_1 when θ is present and absent. Fig. 9 shows the dependence of f_1 on φ_μ for the parameter set B for finite (solid curve) and vanishing (dashed curve) θ in the chargino mass matrix. First one observes the absence of any symmetry in the behaviour of f_1 which is already expected from the interference among various sinus and cosinus functions. The next thing is that away from the CP-conserving points, $[\varphi_\mu = 0, \pi, 2\pi]$, f_1 for vanishing θ dominates and assumes approximately the same value that it gets for finite θ near the CP-conserving points. Assuming that there is no constraint on the range of φ_μ , one observes that the net effect of θ is to push those large CP violation points near CP conserving ones. For instance, $f_1[\varphi_\mu \sim 1.5, \theta = 0] \equiv f_1[\varphi_\mu \sim \pi, \theta \neq 0]$, so that it is just a matter of shift in the value of φ_μ . However, there are counter examples to this conclusion where f_1 for finite θ dominates on the one for vanishing θ . The first example is based on the parameter set C above

whereas the other two are discussed below for the parameter sets D and E . The parameter set C suggests a rather small value for the threshold value of φ_{A_t} compared to the previous sets B and A . Hence one is comparatively closer to the CP conserving point $\varphi_{A_t} = 0$. In this context, Fig. 10 shows the dependence of f_1 on φ_μ for the parameter set C for finite (solid curve) and vanishing (dashed curve) θ . It is obvious that nowhere dashed curve appears, and this stems from the fact that f_1 for vanishing θ is small. To see this better, one may check Fig. 11 where variation of f_1 near $\varphi_\mu = 2\pi$ is shown for finite (solid curve) and vanishing (dashed curve) θ . As the figure suggests f_1 at finite θ is ~ 6 times larger than the one for vanishing θ when the latter attains its maximum. However, one notices that the parameter set C already pushes the non-vanishing f_1 region near a CP-conserving point around which such a dominance is already expected.

In Figs. 5-11 the main interest has been the φ_μ -dependence of f_i for fixed values of the remaining parameters as given in the sets A , B and C . The main conclusion from these examples is the *existence of large CP violation near the CP-conserving points* where f_i , with θ present, can, depending on the parameter space, dominate on the one when θ is absent in certain portions of or everywhere along the φ_μ axis.

The next example to show the dominance of f_i at finite θ over the ones at vanishing θ consists of the variation of f_i with $\tan\beta$ and M_A . For this purpose, it is convenient to introduce two new parameter sets

$$D = \left\{ M_{\tilde{L}} = M_{\tilde{R}} = M_2 = 2 \cdot M_Z, M_A = M_Z, |A_t| = 1.6 \cdot M_Z, \right. \\ \left. |\mu| = 1.6 \cdot M_Z, \varphi_\mu = 0.5, \varphi_{A_t} = 0.5 \right\}, \quad (21)$$

$$E = \left\{ M_{\tilde{L}} = M_{\tilde{R}} = M_2 = 2 \cdot M_Z, M_A = 4 \cdot M_Z, |A_t| = 1.6 \cdot M_Z, \right. \\ \left. |\mu| = 1.6 \cdot M_Z, \varphi_\mu = 0.5, \varphi_{A_t} = 0.5 \right\}. \quad (22)$$

Contrary to Figs. 5-11 in the following figures the constraint $|\sin\theta| \geq 1$ will be relaxed when there is no θ contribution to the chargino mass matrix; namely, the constraints on θ will be just forgotten when analyzing the bare chargino mass matrix. This is motivated by the requirement of observing the relative magnitudes of f_i as a function of $\tan\beta$ when θ is present and absent. Moreover, in the following figures $\tan\beta$ will be varied from 2 to 100 mainly for observing the asymptotic behaviour of the chargino mixings when there

is no θ contribution. However, the derivation θ in eq. (3) [10] assumes the dominance of the top quark and top squark loops, so that graphs of f_i when θ is present could be taken with great *care* for $\tan\beta \gtrsim 40$. In this respect, it is healthy to compare the asymptotic value of f_i for vanishing θ with f_i for finite θ below $\tan\beta \sim 40$.

Depicted in Fig. 12 is $\tan\beta$ -dependence of f_1 for the parameter set D when θ is present (solid curve) and absent (dashed curve) in the chargino mass matrix. For small $\tan\beta$ the two curves are close to each other due to the fact that $|\sin\theta|$ is small. But then, as $\tan\beta$ increases, the solid curve rapidly increases, and becomes twice bigger than the dashed curve. Beyond $\tan\beta \sim 20$ the solid curve vanishes because of the violation of $|\sin\theta|$ constraint in \mathcal{C} . However, as mentioned in the previous paragraph the dashed curve keeps increasing slowly such that even at $\tan\beta = 100$ it remains around its value at $\tan\beta = 2$. In particular, it can never catch the solid curve with such a slow increase. It is seen that $|\sin\theta|$ forces the solid curve to vanish before the validity limit of eq. (3) is violated. Essentially the same thing happens for f_2 in Fig. 13. Additionally, to see the effects of M_A on f_i , one can use the set E in which case $\sin\theta$ in eq. (3) is reduced by a factor of 16 compared to the one in set D . Needless to say, all dashed curves will keep their behaviour in Figs. 12 and 13. In this respect, one can see Figs. 14 and 15 where, in accordance with large M_A value in the set E , the dashed and solid curves get closer at $\tan\beta = 2$. Moreover, the solid curves nowhere vanish because the constraint \mathcal{C} remains unviolated due to large M_A . Even at $\tan\beta = 100$ for dashed curve it is impossible to catch any value of the solid curve below $\tan\beta \sim 40$. Hence the conclusion remains the same as for Figs. 12 and 13. As a result, the study of Figs. 12-15 adds one more conclusion: *value of f_i , when θ is present, remains much larger than the value of f_i when θ is absent, and this gap cannot be closed however large $\tan\beta$ is chosen.*

The analytic as well as the numerical analyses above have been based solely on the chargino sector for simplicity. Of course, the neutralino sector is also important and must be analyzed in detail. The method of discussion in that case proceeds on similar lines with mostly numerical procedures because the neutralinos, which are the mass eigenstates of neutral gauginos and Higgsinos, are described by a 4×4 mass matrix whose analytic treatment is not illuminating. However, just because of the similarity of the mass matrices

in terms of their dependencies on μ parameter and θ [12] one expects similar effects to take place in the case of neutralinos, too. Though not discussed here, effects of the additional phase θ on the neutralino sector are no way negligible, as they are equally important for the phenomena where charginos play a role. After tracing the effects of θ on the chargino sector one infers the neutralino sector be affected by similar ways, and their treatment can be done in discussing the specific processes where neutralinos contribute.

When discussing the Figs. 5-11 importance of proximity to a CP conserving point has been frequently emphasized without an explicit reason. Therefore it may be convenient to have a detailed discussion of it. First, one recalls the situation in minimal supergravity models with finite phases. The phase of the μ parameter remains unchanged, and the phase of the Higgs–sfermion trilinear couplings gets aligned towards that of the gaugino masses during the RGE running from GUT scale to the weak scale. Thus, the A –terms cannot have a large phase after field redefinitions to obtain the physical set of phases, and this remains true unless one chooses the universal gaugino mass much smaller than the universal A –terms at the supergravity scale. On the other hand particle EDM’s constrain the μ parameter severely. In this sense, in minimal supergravity models (see the second reference in [7]) the low energy model is necessarily close to a CP–conserving point. The second reason for being in the vicinity of the CP–conserving points follows from the relaxation property of the pseudo–Goldstone modes of the $U(1)_{PQ}$ and $U(1)_{R-PQ}$ symmetries of the MSSM Lagrangian in a generalization of the Peccei–Quinn mechanism. It has been shown in [2] that these Goldstone modes relax to or near a CP–conserving point leading to a solution of the strong and supersymmetric CP problems by similar mechanisms. Furthermore, specific realizations of these Goldstone modes have already been constructed in dynamical supersymmetry breaking scenarios [4]. One of the major effects of these phases would be the induction of a macroscopic Yukawa-type force between the massive bodies [2] which can be significant for phases $\mathcal{O}(1)$ since the masses of the pseudo–Goldstone modes can lie just above a TeV. In this sense, one expects MSSM be near a CP–conserving point after the general derivation in [2], and thus, *having large CP violation when φ_{A_t} and φ_μ are near a CP–conserving point is important.*

Even if one assumes a typical globally supersymmetric low energy model

with the SM gauge group by just forgetting about the constraints in the previous paragraph, still there are nontrivial effects of the additional phase θ on the phenomena where φ_{A_t} and φ_μ play a role. For example, one recalls the cancellation of different supersymmetric contributions in certain portions of the MSSM parameter space (See the second and third references in [13]) in calculating the EDM's or other FCNC transitions. As the graphs in Figs. 12-15 show clearly, now the $\tan\beta$ -sensitivity of the supersymmetric phases is modified; hence, the constraints on the MSSM parameter space. Another important point deserving discussion concerns the electroweak baryogenesis [8] where the necessary amount of CP-violation could be of explicit or spontaneous [12] in nature though the latter can require an unrealistically small pseudoscalar mass. The observation here is that the relative alignment between the Higgs doublets, even for very small φ_μ and φ_{A_t} , can be large enough to source necessary CP violation for the electroweak baryogenesis.

3 Conclusion

This work has dealt with the induction and subsequent effects of the unremovable alignment between the Higgs doublets due to explicit CP violation in the MSSM Lagrangian. This radiatively induced phase could be as large as the CP phases themselves in easy-to-find portions of the MSSM parameter space as exemplified by Figs. 1-4. This additional phase can affect chargino and neutralino sectors through their mass matrices. In here, for the particular case of charginos, the effects of this phase have been discussed both analytically and numerically. It is shown that this additional phase can induce large CP violation near the CP-conserving points in the chargino sector. Moreover, the CP violation in the presence of this radiatively induced phase is highly sensitive to $\tan\beta$, and larger than the one in the absence of it. Although no discussion of the neutralinos is given, just by the similarity of the mass matrices in terms of their dependence on this extra phase one expects neutralino sector to have similar additional CP violation effects.

Now it is of phenomenological interest to determine the additional CP violation effects on various phenomena where the supersymmetric CP violation effects contribute. For example, an analysis of the neutralino sector together with the results of this work will be important for EDM's of parti-

cles [5], LSP searches [6], K - and B - physics [1, 7], electroweak baryogenesis [8], and weak and electromagnetic dipole formfactors [9]. In particular, for a real CKM matrix [22], the CP-violation in K and B physics [1, 7] follows solely from the chargino and neutralino sectors so that this additional phase θ becomes important there.

4 Acknowledgements

The author is grateful to Antonio Masiero, Mariano Quirós, and Oscar Vives for fruitful discussions.

References

- [1] M. Dugan, B. Grinstein and L. J. Hall, Nucl. Phys. **B255**, 413 (1985).
- [2] S. Dimopoulos and S. Thomas, Nucl. Phys. **B465**, 23 (1996).
- [3] M. Brhlik, L. Everett, G. L. Kane, and J. Lykken, hep-ph/9905215.
- [4] T. Banks, D. Kaplan, and A. Nelson, Phys. Rev. D **49**, 779 (1994); J. Bagger, E. Poppitz, and L. Randall, Nucl. Phys. **B426**, 3 (1994); S. Dimopoulos and L. J. Hall, Phys. Rev. Lett. **60**, 1899 (1988).
- [5] J. Ellis, S. Ferrara and D. V. Nanopoulos Phys. Lett. **114B**, 231 (1982); W. Buchmüller and D. Wyler, *ibid.* **121B**, 321 (1983); J. Polchinski and M. Wise, *ibid.* **125B**, 393 (1983); F. del Aguila, M. Gavela, J. Grifols and A. Mendez, *ibid.* **126B**, 71 (1983); D. V. Nanopoulos and M. Srednicki, *ibid.* **128B**, 61 (1983); Y. Kizukuri and N. Oshimo, Phys. Rev. D **46**, 3025 (1992); T. Falk and K. A. Olive, Phys. Lett. **375B**, 196 (1996); T. Falk, K. A. Olive and M. Srednicki, *ibid.* **354B**, 99 (1995).
- [6] T. Falk, A. Ferstl, and K. A. Olive, Phys. Rev. D **59**, 055009 (1999).
- [7] D. A. Demir, A. Masiero, and O. Vives, Phys. Rev. Lett. **82**, 2447 (1999); T. Goto, Y.Y. Keum, T. Nihei, Y. Okada, and Y. Shimizu, hep-ph/9812369; S. Baek and P. Ko, hep-ph/9904283.
- [8] M. Carena, M. Quiros, A. Riotto, I. Vilja, and C.E.M. Wagner, Nucl. Phys. **B503**, 387 (1994); M. Carena and C.E.M. Wagner, hep-ph/9704347; K. Funakubo, S. Otsuki, and F. Toyoda, hep-ph/9903276; J. Cline, M. Joyce, and K. Kainulainen, Phys. Lett. **417B** (1998) 79; M. Laine and K. Rummukainen, hep-ph/9811369; K. Funakubo, hep-ph/9809517; K. Funakubo, A. Kakuto, and F. Toyoda, Prog. Theor. Phys. **96**, 771 (1996).
- [9] W. Hollik, J.I. Illana, C. Schappacher, D. Stockinger, and S. Rigolin, hep-ph/9808408; W. Hollik, J.I. Illana, S. Rigolin, C. Schappacher, and D. Stockinger, hep-ph/9812298.
- [10] D. A. Demir, hep-ph/9901389 (to appear in Phys. Rev. D).

- [11] A. Pilaftsis and C. E. M. Wagner, hep-ph/9902371 (to appear in Nucl. Phys. B); D. A. Demir, hep-ph/9809360; A. Pilaftsis, Phys. Rev. D **58**, 096010 (1998); Phys. Lett. **435B**, 88 (1998).
- [12] G. C. Branco and M. N. Rebelo, Phys. Lett. **160B**, 117 (1985); K. Funakubo, A. Kakuto, S. Otsuki, and F. Toyoda, Prog. Theor. Phys. **99**, 1045 (1998); J. Liu and L. Wolfenstein, Nucl. Phys. **B289**, 1 (1987); N. Maekawa, Phys. Lett. **282B**, 387 (1992).
- [13] S. A. Abel and J. M. Frere, Phys. Rev. D **55**, 1623 (1997); T. Ibrahim and P. Nath, *ibid.* **57**, 478 (1998); *ibid.* **58** (1998) 111301; M. Brhlik, G. J. Good and G. L. Kane, hep-ph/9810457; S. Dimopoulos and G. F. Giudice, Phys. Lett. **357B**, 573 (1995); A. Cohen, D. B. Kaplan and A. E. Nelson, Phys. Lett. **388B**, 599 (1996); A. Pomarol and D. Tommasini, Nucl. Phys. **B488**, 3 (1996).
- [14] M. Sher, Phys. Rep. **179**, 273 (1989).
- [15] H. E. Haber and R. Hempfling, Phys. Rev. Lett. **66**, 1815 (1991); A. Yamada, Phys. Lett. **263B**, 233 (1991); P.H. Chankowski, S. Pokorski and J. Rosiek, *ibid.* **274B**, 191 (1992).
- [16] Y. Okada, M. Yamaguchi and T. Yanagida, Prog. Theor. Phys. **85**, 1 (1991); J. Ellis, G. Ridolfi and F. Zwirner, Phys. Lett. **257B**, 83 (1991), and *ibid.* **262B**, 477 (1991); R. Barbieri and M. Frigeni, *ibid.* **258B**, 395 (1991); A. Brignole, J. Ellis, G. Ridolfi and F. Zwirner, *ibid.* **271B**, 123 (1991); A. Brignole, *ibid.* **281B**, 284 (1992).
- [17] Y. Okada, M. Yamaguchi and T. Yanagida, Phys. Lett. **262B**, 54 (1991); R. Barbieri, M. Frigeni and F. Caravaglios, *ibid.* **258B**, 167 (1991); J.R. Espinosa and M. Quirós, *ibid.* **266B**, 389 (1991); J. Kodaira, Y. Yasui and K. Sasaki, Phys. Rev. D **50**, 7035 (1994); R. Hempfling and A.H. Hoang, Phys. Lett. **331B**, 99 (1994); J.A. Casas, J.R. Espinosa, M. Quirós and A. Riotto, Nucl. Phys. **436B**, 3 (1995); (E) **B439**, 466 (1995); M. Carena, J.R. Espinosa, M. Quirós and C.E.M. Wagner, Phys. Lett. **355B**, 209 (1995); M. Carena, M. Quirós and C.E.M. Wagner, Nucl. Phys. **B461**, 407 (1996); H.E. Haber, R. Hempfling and A.H. Hoang, Z. Phys. **C75**, 539 (1997); S. Heinemeyer, W. Hollik and G. Weiglein, Phys. Rev. D **58**, 091701 (1998); hep-ph/9903404.

- [18] M. Bando, T. Kugo, N. Maekawa, and H. Nakano, Mod. Phys. Lett. **A7**, 3379 (1992).
- [19] H. E. Haber, hep-ph/9505240; hep-ph/9806331; hep-ph/9901365.
- [20] J. A. Casas, A. Lleyda, and C. Munoz, Nucl. Phys. **B471**, 3 (1996).
- [21] H. E. Haber and G. L. Kane, Phys. Rep. **117**, 75 (1985).
- [22] G.C. Branco, F. Cagarrinho, and F. Kruger, hep-ph/9904379.
- [23] M. Aoki, G.-C. Cho, and N. Oshimo, hep-ph/9903385.
- [24] G. C. Branco, G.-C. Cho, Y. Kizukuri, and N. Oshimo, Nucl. Phys. **B449**, 483 (1995).

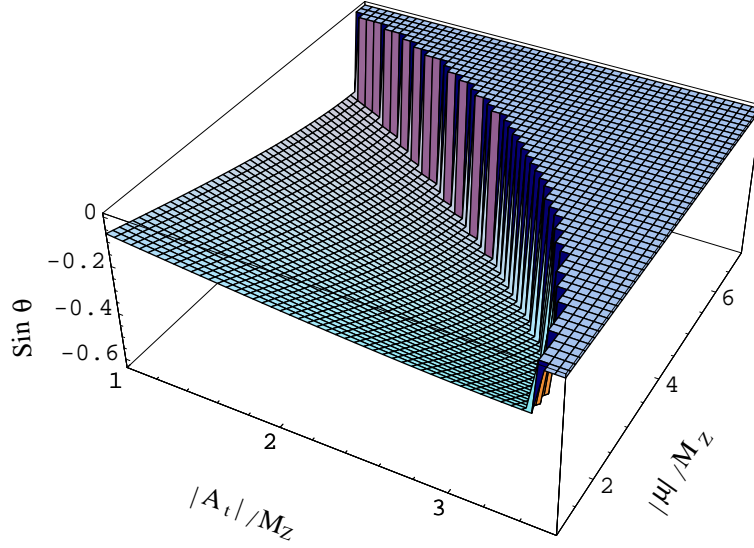


Figure 1: $\sin \theta$ in $|A_t|/M_Z - |\mu|/M_Z$ plane for $\tan \beta = 2$ and $M_A = M_Z$. The $\sin \theta = 0$ plateau *is not* the value of $\sin \theta$; it shows just the parameter region *excluded* by either $m_{\tilde{t}_1} < M_Z$ or $|\sin \theta| > 1$.

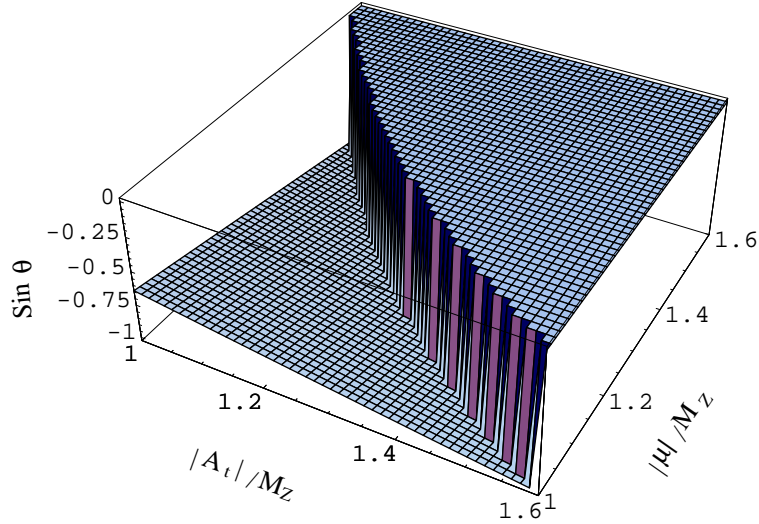


Figure 2: The same as in Fig. 1, but for $M_A = M_Z$ and $\tan \beta = 30$.

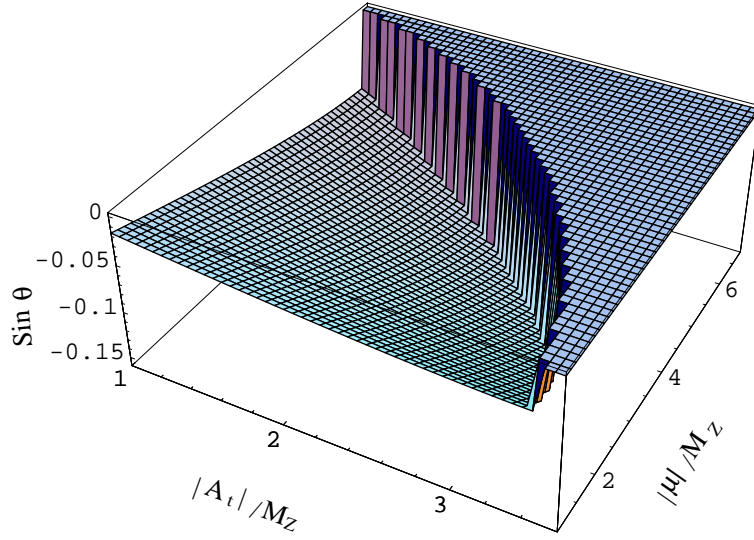


Figure 3: The same as in Fig. 1, but for $M_A = 2 \cdot M_Z$ and $\tan \beta = 2$.

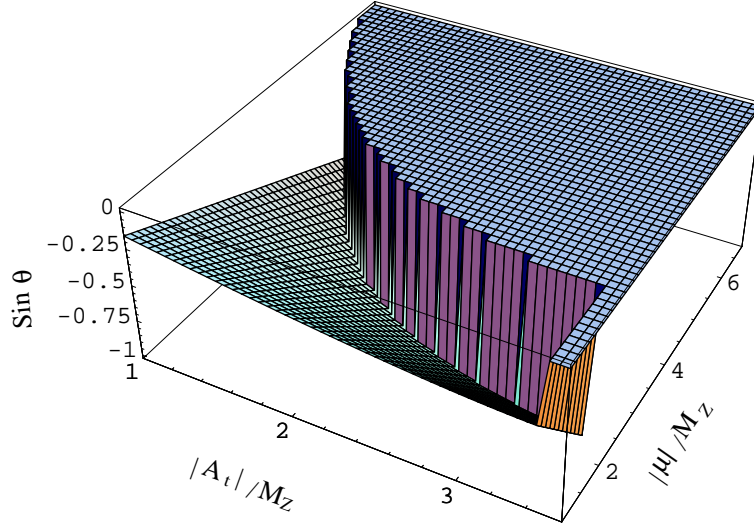


Figure 4: The same as in Fig. 1, but for $M_A = 2 \cdot M_Z$ and $\tan \beta = 30$.

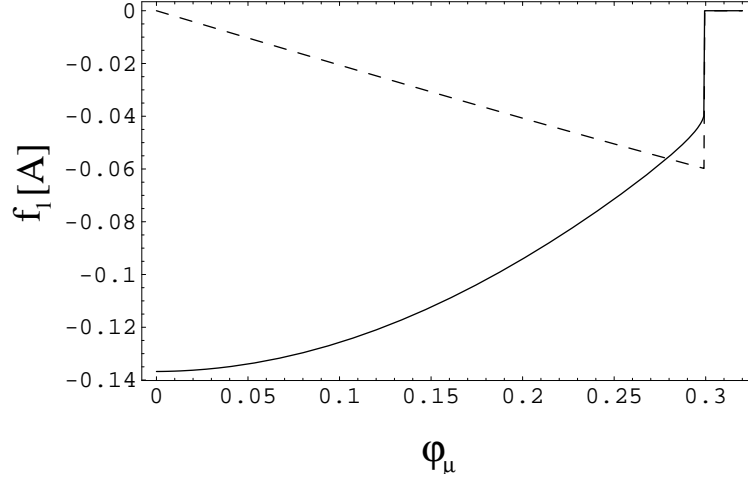


Figure 5: The dependence of f_1 on φ_μ for the parameter set A .

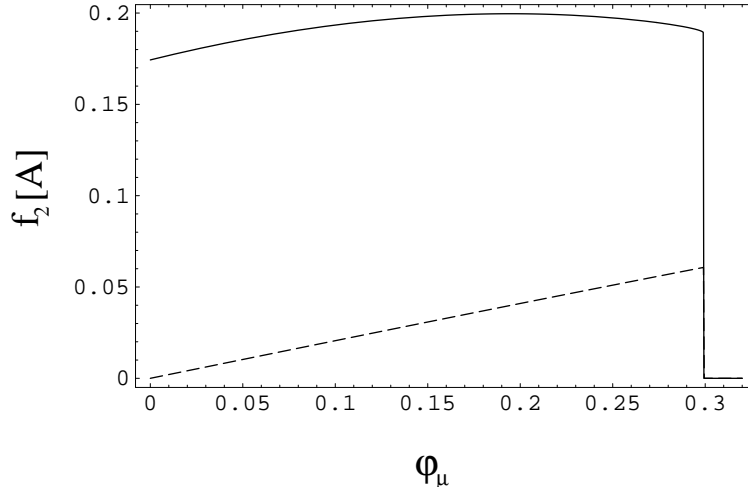


Figure 6: The dependence of f_2 on φ_μ for the parameter set A .

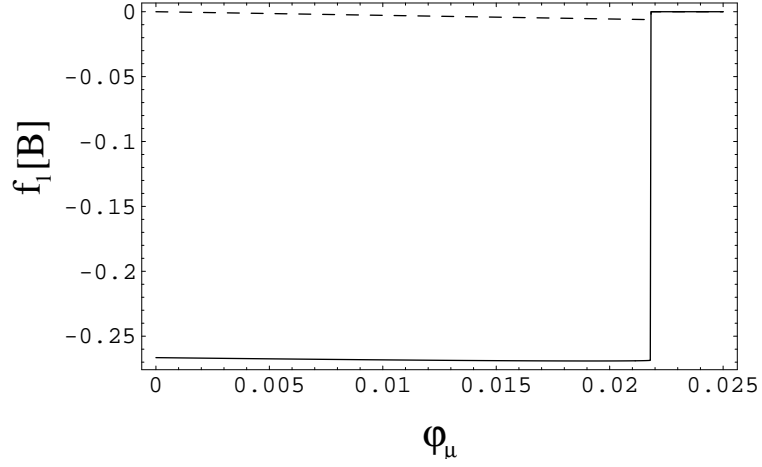


Figure 7: The dependence of f_1 on φ_μ for the parameter set B .

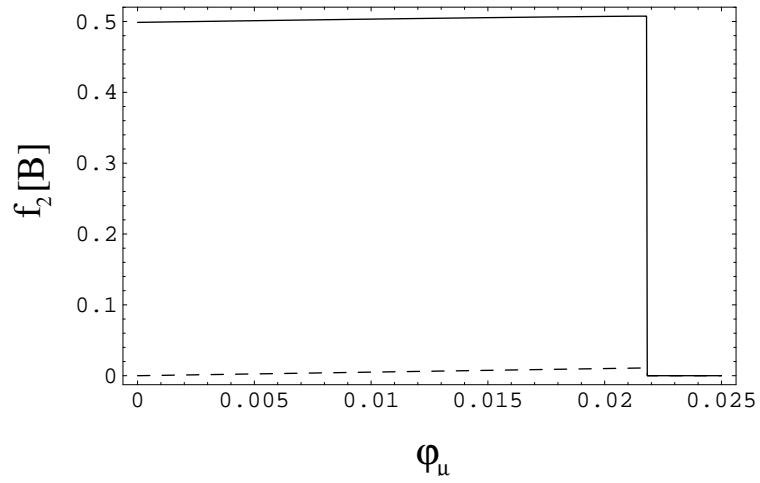


Figure 8: The dependence of f_2 on φ_μ for the parameter set B .

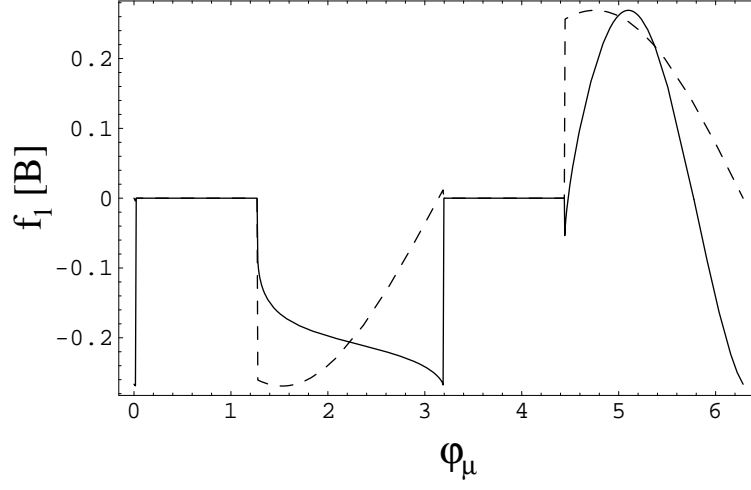


Figure 9: f_1 for the parameter set B in the entire range of φ_μ .

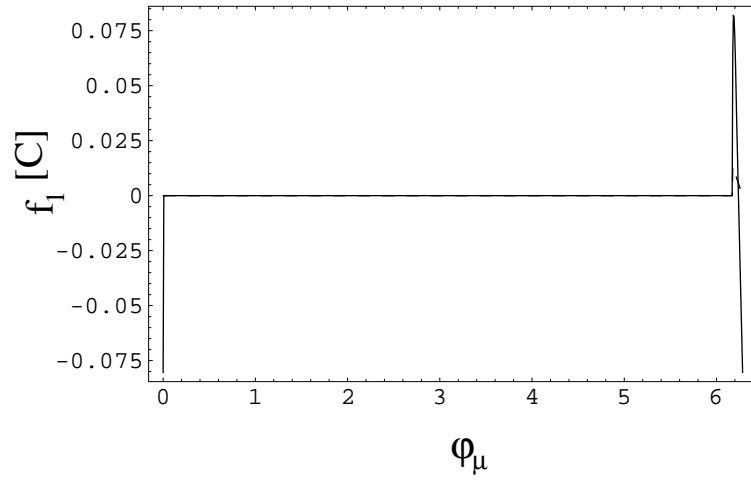


Figure 10: f_1 for the parameter set C in the entire range of φ_μ .

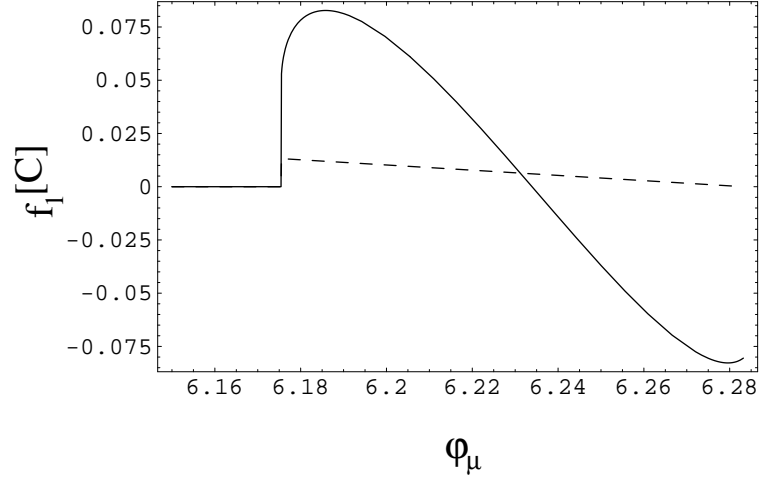


Figure 11: f_1 for the parameter set C in the vicinity of $\varphi_\mu = 2\pi$.

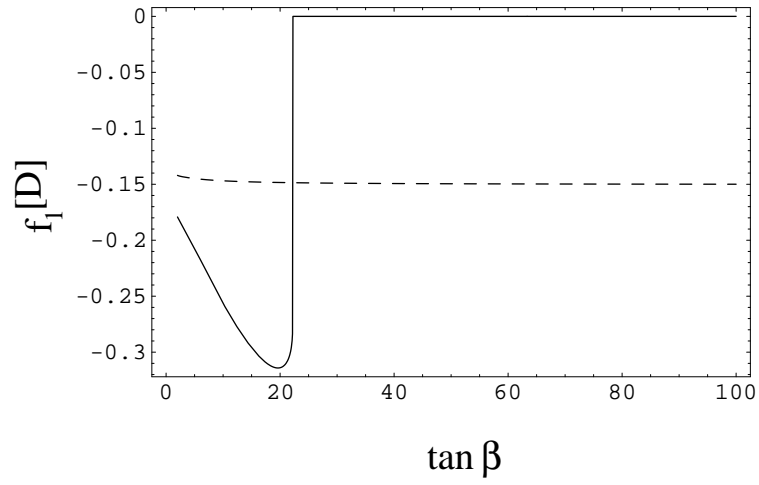


Figure 12: Variation of f_1 with $\tan \beta$ for the parameter set D .

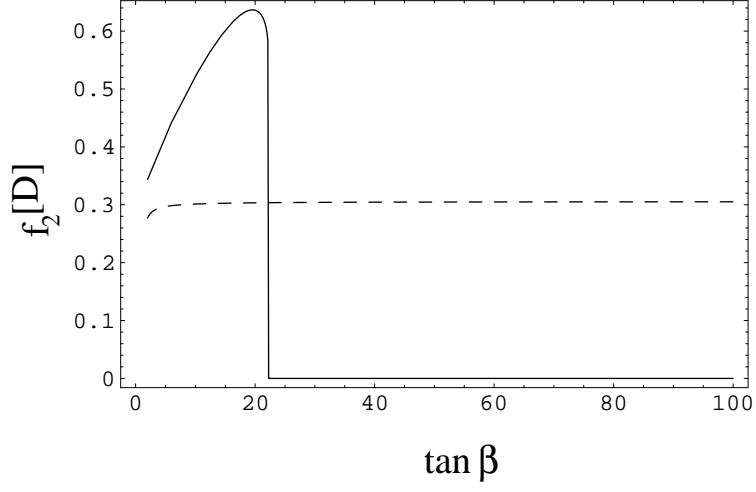


Figure 13: Variation of f_2 with $\tan \beta$ for the parameter set D .

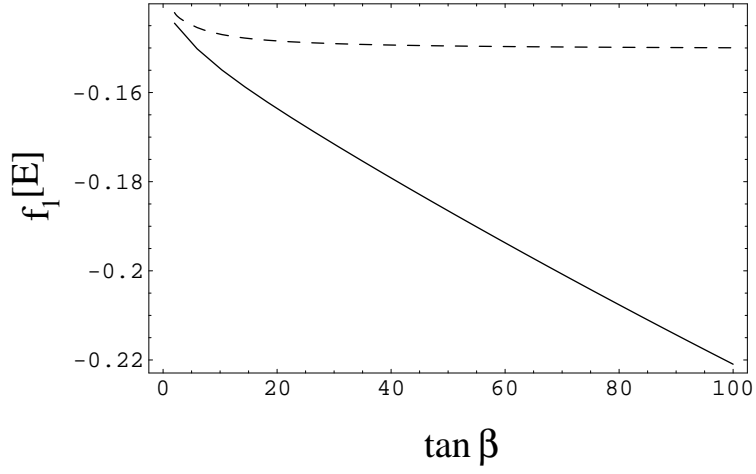


Figure 14: Variation of f_1 with $\tan \beta$ for the parameter set E .

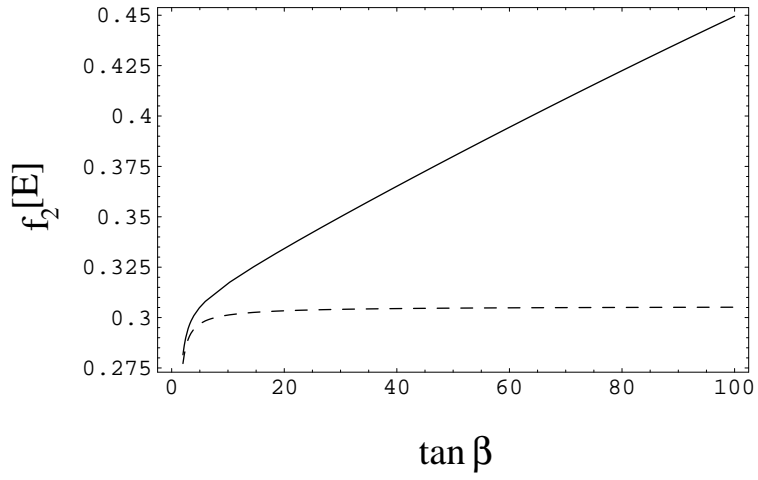


Figure 15: Variation of f_2 with $\tan \beta$ for the parameter set E .